Analyst

ROYAL SOCIETY OF CHEMISTRY

PAPER

View Article Online
View Journal | View Issue

Cite this: *Analyst*, 2022, **147**, 5306

Development of a PNA–$DiSc_2$ based portable absorbance platform for the detection of pathogen nucleic acids†

Shailesh B. Lad,‡[a] Shomdutta Roy,‡[a] Jijo Easo George,[a] Himadri Chakraborti,[b] Saumitra Lalsare,[a] Bikash Barik,[b] Arushi Singh,[b] Amrutraj Zade,[c] Sachee Agrawal,[d] Jayanthi Shastri,[d] Anirvan Chatterjee,[c] Kantimay Das Gupta,[b] Debjani Paul *[a] and Kiran Kondabagil *[a]

We report the development of a portable absorption (PortAbs)-based pathogen nucleic acid detection system using peptide nucleic acid (PNA) and a cyanine dye, $DiSc_2(5)$. When the dye binds to the PNA–DNA hybrid, it results in a characteristic ~110 nm shift in the dye absorbance, which we measure using PortAbs. The protocol involves amplification of the target DNA, PNA–DNA hybridization and dye complexing steps followed by absorption measurement. The system is built using a broad-spectrum photodiode whose output is amplified and then measured by a high resolution (24 or 32 bit) analog-to-digital converter. The excitation pulses of light are delivered by a color-changing LED. The sequence of excitation, measurement and display of results are all controlled by an embedded Raspberry-Pi board (or alternatively a laptop). At higher concentrations of the target amplicon (~200 ng), the color change can be detected visually. At lower concentrations, PortAbs outperforms a plate reader and can detect target DNA as low as 30 ng or approximately 10 nM which is at least 10 fold better than previously reported studies. We validate the methodology using SARS-CoV-2 clinical samples containing about 1000 copies of the viral RNA and show that the entire workflow takes about 90 min. The cost of the complete standalone system is less than INR 40 000 (approx. 500 USD).

Received 16th August 2022,
Accepted 23rd October 2022

DOI: 10.1039/d2an01351g

rsc.li/analyst

Introduction

Real-Time quantitative PCR (RT-qPCR) has transformed the field of clinical microbiology by providing a precise and rapid method for the detection and quantification of pathogens.[1] Prior to the invention of RT-qPCR, classical culture-based methods coupled with biochemical analysis were used for the identification of pathogens. Such methods may require several days to weeks for successful identification and diagnosis. The high sensitivity and specificity of the RT-qPCR method has made it one of the most widely used confirmatory tests for detection of pathogens. Naturally, during the COVID-19 pandemic, RT-qPCR has been deployed widely across the world for the detection of SARS-CoV-2 RNA.[2,3] Despite its advantages, the method suffers from certain drawbacks including the requirement of expensive instruments and reagents, in addition to trained personnel. In the last 24 months, several attempts have been made to find alternative cost-effective methodologies that could complement RT-qPCR for mass scale testing. Apart from the RT-qPCR, other nucleic acid-based diagnostic tests include SHERLOCK,[4] FELUDA,[5] and DETECTR,[6] which employ the CRISPR technology for the detection of SARS-CoV-2 RNA. Despite their high sensitivity and specificity, the limited availability of enzymes used for these assays constrains their widespread use. Several immunoassays have also been developed for the rapid detection of SARS-CoV-2.[7,8] Such assays rely on the detection of viral antigens like structural proteins or virus-induced host antibodies. Immunoassays have also been used for the development of biosensors.[9] Although such tests are relatively inexpensive and rapid, their major drawback is the variation of antigen/antibody titers during the course of infection which can lead to false-negative outputs. Thus, due to the high specificity and sensitivity of nucleic acid-based detection

[a]*Department of Biosciences and Bioengineering, Indian Institute of Technology Bombay, Powai, Mumbai, India. E-mail: kirankondabagil@iitb.ac.in, debjani.paul@iitb.ac.in*
[b]*Department of Physics, Indian Institute of Technology Bombay, Powai, Mumbai, India*
[c]*Haystack Analytics Pvt. Ltd. Society For Innovation & Entrepreneurship (SINE), Kanwal Rekhi Building, Indian Institute of Technology Bombay, Powai, Mumbai, India*
[d]*Molecular Diagnostic Reference Laboratory, Kasturba Hospital for Infectious Diseases, Mumbai, India*

†Electronic supplementary information (ESI) available. See DOI: https://doi.org/10.1039/d2an01351g

‡Equal contribution.

tests, there is a requirement for developing additional cost-effective and simpler methods that can be deployed widely in resource-constrained settings for the detection and surveillance of pathogens.

Peptide nucleic acid (PNA) is a nucleic acid analogue containing nucleobases attached to an uncharged polyamide backbone.[10,11] PNA forms stable Watson–Crick hydrogen bonding with a complementary PNA, DNA, or RNA sequence and can be used as a highly specific probe for the detection of nucleic acids. The initial use of PNA to recognize a DNA sequence was mainly based on the change in the fluorescence intensity and/or polarization upon binding of a modified base-containing PNA to a complementary DNA.[12] Another method to detect PNA–DNA hybridization is based on the affinity of cyanine dyes to a PNA–DNA duplex.[13] This binding is primarily driven by the hydrophobic and van der Waals interactions leading to a change in the spectral properties of the dye.[13,14] For instance, the free cyanine dye 3,3′-diethylthiadicarbocyanine [$DiSc_2(5)$] (Fig. 1A) exhibits a characteristic absorption spectrum with peaks at 580 nm and 650 nm which show a blue-shift to ~540 nm upon binding to a DNA–PNA hybrid. This shift in absorbance leads to a distinct color change from blue to purple, thereby providing a visual indicator of hybridization (Fig. 1B). The stability of PNA, coupled with the ease of detecting the color change of cyanine dye, has found applications in molecular biology and diagnostics including the detection of single nucleotide polymorphisms.[15–18] However, high amounts of the template DNA are needed for visual detection of the color change. Further, $DiSc_2(5)$ has a tendency to aggregate on PNA strands alone or on partially complementary DNA–PNA hybrids which also leads to a change in the absorption spectrum and could result in false-positive detection of the target DNA.

Earlier studies have reported the development of colorimetric devices for the detection of DNA/RNA. But they employ a smartphone or a digital camera to capture the color change followed by image analysis.[19,20] Duy *et al.* (2014) reported a handheld colorimeter for detection of rRNA using a PNA probe and a cyanine dye.[18] The lowest concentration of RNA they could detect is 100 nM which is ten-folds higher than what we can detect (10 nM). Xu *et al.* (2020) reported a PNA–DNA_2-based colorimetric sensor for detection of miRNA.[21] Their detection is based on a DNA–RNA hybrid, the formation of which disassociates the PNA–DNA_2 triplex. In contrast, our detection principle lies on the formation of the PNA–DNA duplex. PNA–DNA is known to be more stable than DNA–RNA or DNA–DNA duplexes due to the neutral backbone of PNA compared to the negatively charged backbones of DNA and RNA, which may induce some electrostatic repulsion between the two strands. Wang *et al.* (2009)[22] reported accelerated photobleaching of a cyanine dye in the presence of DNA–PNA–dye triplex, which can be used as a diagnostic tool for detection of infectious pathogens. As this method requires alternate rapid exposure to light (470 nm) and darkness for accelerated photobleaching of the dye, it needs a 470 nm light source in addition to the absorption measurement unit. This may reduce the applicability of this method in point-of-care settings.

We report an easy-to-use and portable diagnostic system for SARS-CoV-2 based on the formation of DNA–PNA–$DiSc_2(5)$ trimeric complex. Our absorption-based detection system relies on the spectral shift of the $DiSc_2(5)$ dye from blue to purple upon binding to a PNA–DNA duplex which is then detected using PortAbs- a sensitive and portable absorption measurement platform without any moving parts that has been developed by us. We demonstrate the specificity of our technique by distinguishing between SARS-CoV-2 and other respiratory pathogens while detecting low amounts of DNA. To the best of our knowledge, PortAbs can detect DNA concentrations about ten times lower than previously reported PNA–$DiSc_2(5)$ based methods which use about 100 nM to few micromolar DNA.[16,17,23,24] Additionally, we address the problem of non-specific aggregation of $DiSc_2(5)$ dye on PNA alone and suggest some possible solutions to mitigate this effect. Finally, we validate this technique against the RT-qPCR detection system using nasopharyngeal samples from individuals suffering from COVID-19. In summary, we have developed an integrated, portable, field-deployable, and low-cost platform for the detection of pathogens that eliminates the need for sophisticated RT-qPCR instruments. While we have demonstrated its performance using SARS-CoV-2 as an example, this platform can be deployed for testing and surveillance of viral pathogens in the environment, testing of food samples, water quality monitoring, *etc*.

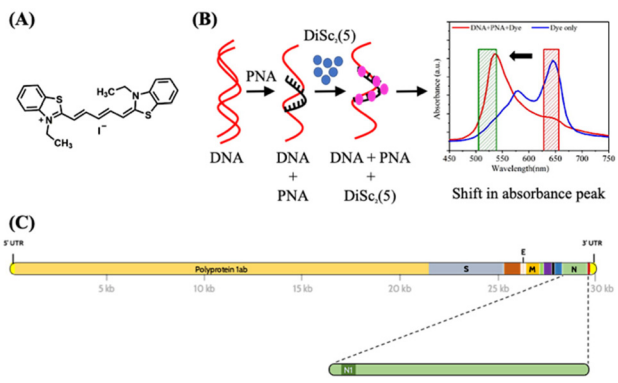

Fig. 1 Schematic diagram showing the PNA–dye based detection assay. (A) Chemical structure of 3,3′-diethylthiadicarbocyanine dye [$DiSc_2(5)$]. (B) Formation of the DNA–PNA–$DiSc_2(5)$ complex leads to a ~110 nm shift in the absorbance peak from red (650 nm) to green (540 nm). (C) Schematic representation of the SARS-CoV-2 genome architecture showing the spike (S), envelope (E), membrane (M) and the nucleocapsid (N) genes. A subset of the N1 fragment of the nucleocapsid gene is the target for our custom designed PNA.

Materials and methods

PCR amplification of target gene

As recommended by the Centers for Disease Control and Prevention (CDC), we targeted the N1 gene fragment (72 bp) from the nucleocapsid gene of SARS-CoV-2 (Fig. 1C). It was amplified using a control plasmid (IDT, Catalogue no.

10006625) as the template (1×10^5 copies), 500 nM each of the N1 forward primer (5′-GACCCCAAAATCAGCGAAAT-3′) and N1 reverse primer (5′-TCTGGTTACTGCCAGTTGAATCTG-3′) and 2× PCR master mix (Thermo Fisher Scientific). PCR was performed on a thermal cycler (MJ mini, Bio-Rad Laboratories or the miniPCR®) using an initial denaturation step at 95 °C for 3 min, followed by 35 cycles (95 °C for 30 s, 60 °C for 30 s and 72 °C for 30 s) and a final extension step at 72 °C for 10 min. The presence of the amplicon was confirmed by 4% agarose gel electrophoresis and the amplified DNA was quantified using the NanoDrop™ Lite Spectrophotometer (Thermo Fisher Scientific).

Detection of the amplicon

The DNA–PNA detection scheme was based on the protocol suggested by Wilhelmsson *et al.* (2002).[16] The N1 gene was amplified following the protocol described earlier. A 15-bases long PNA sequence (5′-CATTACGTTTGGTGG-Lysine–Lysine-3′) complementary to the N1 probe region (Fig. 1C) was custom synthesized (Panagene Incorporation, South Korea or Creative Biomart Inc., USA). The presence of two lysine residues at the 3′ end of the PNA sequence improve its solubility in aqueous buffers.[15,22,25] The PCR products were either used directly for PNA binding or purified using a QIAquick® gel extraction kit (Qiagen) to remove the unused dNTPs, salts, and other components of the PCR master mix solution before binding to the PNA. The amplified DNA was mixed with 0.7 μL of PNA (1 μM final concentration) and phosphate buffered saline (pH 7.4) to a final volume of 70 μL. For the initial optimization process, three different concentrations of PNA (1, 5, and 10 μM) were used. The mixture was heated to 95 °C for 5 min in a heat block and incubated at room temperature for 15 min to allow PNA–DNA hybridization. Unless mentioned otherwise, $DiSC_2(5)$ (Sigma Aldrich) dye was added to the PNA–DNA reaction to achieve a final concentration of 25 μM and the reaction mixture was heated again to 95 °C for 2 min to allow the formation of PNA–DNA–dye complex. The absorption spectra were recorded between 450 nm to 750 nm using either the MultiskanGO microplate spectrophotometer (Thermo Fisher Scientific) or the custom-built system (PortAbs).

Components and variants of the PortAbs system

We designed and fabricated a portable absorption system (PortAbs). The RGB LED and the Op-Amps (OP07) were purchased locally. The PIN photodiode (PIN-10DP) was bought from OSI Optoelectronics and an optical fiber coupler (Toslink-RT-2P) was bought from Tobo Digital. The 24-bit Analog-to-Digital converter (ADC) NI9238 (range ± 500 mV) was sourced from National Instruments. A 20 cm × 20 cm light-tight box housing all electronic and optical components was 3D printed in polylactic acid (PLA) using a MakerBot Replicator. The ADC and the excitation LEDs were interfaced with a PC/Laptop running LabView software. Alternatively, we have also made an equivalent measurement system using a 32-bit ADC (Waveshare ADS1263) interfaced to an embedded Raspberry Pi board, taking user input *via* a 4 × 4 matrix keypad. The Raspberry-Pi was programmed in Python. This version is a standalone tabletop instrument adapted for use in field/at point-of-care, whereas the PC based system is more suitable for a laboratory environment.

Determining the sensitivity and specificity

The detection workflow for the PortAbs set-up was identical to the one used for detection using the commercial plate reader (see above) except that the samples were placed in a disposable micro-cuvette. We evaluated the detection limit in PortAbs by successively diluting the template DNA from ~160 ng to ~15 ng. The specificity of our method was established by amplifying DNA from other respiratory pathogens like *Mycobacterium tuberculosis* (Mtb) and MERS-CoV using primers targeted to the N1 gene of SARS-CoV-2. We used the genomic DNA of Mtb, a separate plasmid containing the N gene from MERS-CoV (IDT, Catalogue no. 10006623) and a synthetic RNA (EURM019, Sigma-Aldrich) containing S gene (RBD) of SARS-CoV-2 as control templates. PCR was performed following the amplification protocol for N1 gene of SARS-CoV-2 and the products were hybridized to the PNA sequence complementary to the N1 gene. All reactions were performed in triplicates and detected by both gel electrophoresis and PortAbs.

Validation of the detection system using COVID-19 clinical samples

RNA isolated from leftover nasopharyngeal swab samples of six patients (P3–P8) suffering from COVID-19 were obtained from Kasturba Hospital, Mumbai. For individual samples, two microliters of RNA was used as the template for cDNA synthesis using the iScript cDNA synthesis kit (Bio-Rad Laboratories). The samples were initially validated for the presence of SARS-CoV-2 RNA by mixing 3 μL of cDNA with N1 primer-probe set (IDT) and the GoTaq probe one-step RT-qPCR system (Promega). For detection using PortAbs, an equal volume (3 μL) of the cDNA was used for the amplification of either the N1 gene as described earlier or the spike (S) gene using the following primers: S forward primer (5′-GACATACCCATTGGTGCAGG-3′) and S reverse primer (5′-TGACTAGCTACACTACGTGCC-3′). The amplified products for N1 and spike (S) genes were purified as described earlier. For comparison of the detection limit in PortAbs with RT-qPCR, 3 μL of cDNA was mixed with Brilliant III Ultra-Fast SYBR® Green QPCR master mix (Agilent) and the corresponding primers for N1 and S genes. The C_t values obtained for N1 and S genes for each patient sample were compared with the absorbance measurements obtained from PortAbs. In all the above experiments, no template control (containing nuclease free water) served as the negative control.

Results and discussion

Understanding the effect of dye–PNA concentrations on detection of DNA

The binding of the cyanine dye $DiSc_2(5)$ to PNA–DNA or PNA–RNA hybrids results in a distinct peak at ~540 nm with a

corresponding decrease in the peak at 650 nm (Fig. 1A). PNA is often tagged with amino acids like glycine or lysine to prevent self-aggregation and enhance its solubility in aqueous buffers.[15,16,22,25] Despite its higher affinity for a DNA–PNA duplex, the dye can also aggregate on only DNA[16] or PNA strands. As previously observed, binding of the dye to PNA alone can also lead to a significant increase in the absorption at 540 nm, thereby reducing the sensitivity of the detection method.[17] To use the $DiSc_2(5)$–PNA based method as an indicator of PNA–DNA hybridization, it is essential to reduce the background absorbance produced by the PNA–dye binding. To determine the optimum ratio of dye and PNA, we varied the concentrations of PNA (1, 5, and 10 μM) and $DiSc_2(5)$ dye (5, 25, and 70 μM) in the absence of any DNA. It was difficult to distinguish the lowest concentration of the dye (5 μM) from the background [Fig. 2A, (i)]. Increasing the dye concentration to 25 μM and subsequently to 70 μM led to the formation of characteristic dye peaks at 650 nm and ~570 nm which represent the monomeric and aggregated forms of the dye, respectively [Fig. 2A, (ii and iii)]. Next, we explored how PNA concentration affects the peak at 540 nm. PNA concentrations of 5 and 10 μM led to a peak at 540 nm. Since this PNA–dye peak would overlap with the expected peak due to PNA–DNA–$DiSc_2(5)$ binding [Fig. 2A, (ii and iii)], it became evident that any concentration of PNA beyond 1 μM should not be implemented for the detection of a complementary DNA strand. Hence, all subsequent experiments were performed with the combination of 1 μM PNA and 25 μM dye.

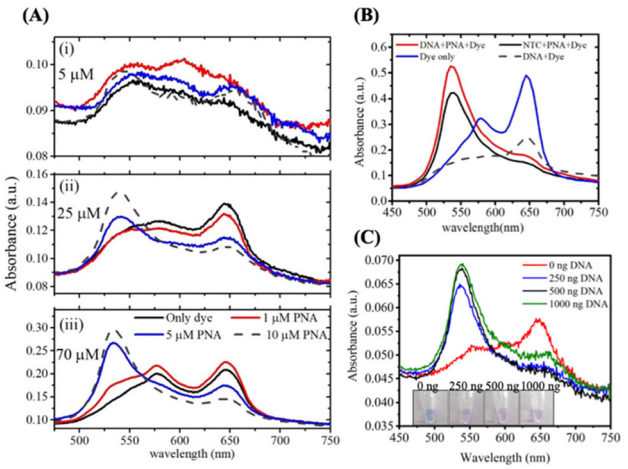

Fig. 2 Optimization of the dye and PNA concentrations for detection. (A) Absorption spectra in presence of 5, 25, and 75 μM $DiSc_2(5)$ respectively. The concentration of PNA varied from 1, 5, and 10 μM in each of these reactions. (B) Absorption spectra of $DiSc_2(5)$ alone (blue line), $DiSc_2(5)$ bound to PNA (solid black line), $DiSc_2(5)$ bound to DNA (dashed black line) and $DiSc_2(5)$–DNA–PNA complex (red line). (C) Absorbance spectra of $DiSc_2(5)$–DNA–PNA complex (N1) after column purification of the PCR product. The photo in the inset confirms that the color change is difficult to distinguish visually when the DNA concentration is low. NTC indicates a no-template control in PCR.

Eliminating non-specific shift in absorption of $DiSc_2(5)$ dye

We next checked the ability of the dye to bind specifically to a PNA–DNA duplex and produce a color change that can be visually detected. We amplified a 72 bp fragment of the N1 gene of SARS-CoV-2, and then allowed the PCR product to bind to the PNA and $DiSc_2(5)$ dye without any purification. The color change upon addition of the $DiSc_2(5)$ dye was used as an indicator of successful hybridization (Fig. 1A). At the dye–PNA concentrations optimized previously (Fig. 2A), we observed a clear increase in the absorbance of the dye at 540 nm (Fig. 2B). This increase followed the common mechanism of dye binding to PNA–DNA heterodimers as described in Fig. 1A. Although unexpected, an increase in the absorbance was also seen in the reaction mixture containing only the PNA probe and the no template control (NTC) consisting of the PCR master mix and the primers (Fig. 2B). To address this non-specific absorbance, we purified the PCR-amplified DNA using a silica-based spin column. We noted a slight increase in the 540 nm peak with an increase in the concentration of the purified target DNA from 250 ng to 1000 ng. The NTC did not show any peak at 540 nm (Fig. 2C). The color of the reaction changed from blue to purple for all concentrations of the template DNA (Fig. 2C, inset).

Our results indicate that the presence of single stranded DNA (unused primers), free dNTPs, and salts (*e.g.*, Mg^{2+}) from PCR leads to non-specific absorbance at 540 nm. A rapid DNA purification step to remove the interfering components can help in improving the specificity of the detection method. While all previous reports have simply compared the absorption spectra of "only dye" and the PNA–DNA–dye complex, this is the first report that highlights the potential interference due to the interaction of $DiSc_2(5)$ dye and the components of the PCR master mix, and suggests a way to minimize this problem.

Development of the PortAbs detection system

As shown in Fig. 3, we developed a portable two-color absorption system that we call PortAbs. Fig. 3A shows the electronic circuit of the detection system. Light from a RGB LED is modulated and passed *via* a fiber-optic coupler to a micro-cuvette containing the sample. The RGB LED emits three wavelengths peaked at 469 nm (blue), 522 nm (green), and 643 nm (red) (Fig. 3C, inset). The wavelength spread of the light from the LED is ~25 nm. Here, we use red and green wavelengths of the LED since these match with the absorption peaks of $DiSc_2(5)$. The light transmitted by the sample is detected by a PIN photodiode. The resulting photocurrent is amplified by a transimpedance amplifier and recorded after digitization of the voltage by the ADC. We were able to detect approximately 1 part in 10^3 change in absorption.

The principle behind the detection system relies on the difference in absorption (α) of the sample in red and green wavelengths. When light of a particular intensity falls on a photodiode, it generates a proportional electric current. A fiber optic coupler is used to channel the light from the LED to the

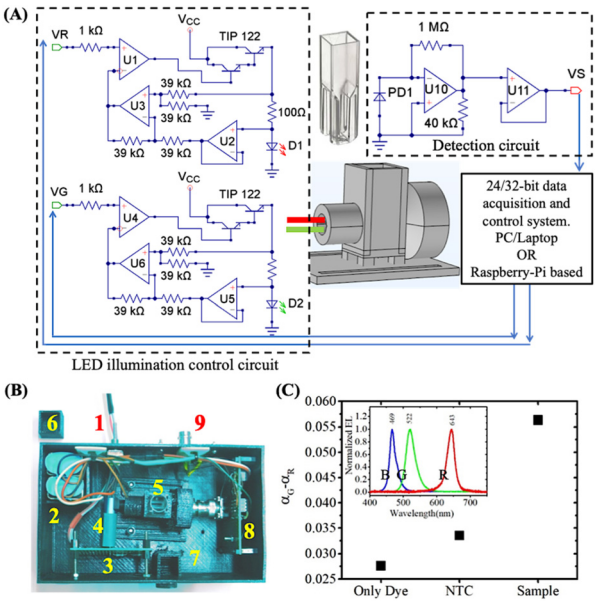

Fig. 3 Custom developed portable absorption set-up, PortAbs. (A) Working principle of the device with photodiode (PD1) based detection and LED intensity control circuit. The Op-Amps U1-U6 are LM324 type, U10-U11 are OP-07. The data acquisition and control system is a laptop running LabView which interfaces with a 24 bit analog-to-digital data acquisition card and a voltage output card. The LEDs are controlled by voltages (VR and VG) for the red and green segments of the RGB LED. (B) A photograph showing the top-view of the PortAbs system: (1) wiring for input control signal, (2) two 9 V batteries, (3) RGB LED, (4) right-angled optical fiber coupler, (5) cuvette, (6) cuvette cap to block stray light, (7) photodiode, (8) current amplifier, (9) output signal to data acquisition system, (C) difference in absorbance of the dye in the green and red wavelengths ($\alpha_G - \alpha_R$) measured for dye alone, dye and PNA in absence of DNA (NTC) and the dye–DNA–PNA complex. The inset shows the wavelength range over which the LED emits.

window of the micro-cuvette. The PIN photodiode detects the transmitted fraction. To eliminate the background signal, the LED is turned on and off under software control several times and the dark current is continuously tracked and subtracted from the signal. The photocurrent is converted to a voltage by a transimpedance amplifier and the output is read by the ADC.

Mathematically, the voltage (V) developed at the detector depends on the intensity of the light (I), the sensitivity of the photodiode (S), and transmittance (t) of the sample between the light source and the photodiode. The sensitivity of the photodiode is a function of wavelength. Initially, the output voltage for green (V_{G0}) and red (V_{R0}) lights are measured with a cuvette filled with DI water (blank), for which $t \approx 1$

$$\begin{aligned} V_{R0} &= S_R I_{R0} \\ V_{G0} &= S_G I_{G0}. \end{aligned} \tag{1}$$

When water is replaced by the sample, which has a transmittance t_G and t_R for green and red wavelengths respectively, we have $\alpha + t = 1$ (since the sum of absorbed and transmitted fractions at any wavelength must be 1). Hence, the output voltage can be written as:

$$\begin{aligned} V_G &= S_G t_G I_{G0} = (1 - \alpha_G) S_G I_{G0} \\ V_R &= S_R t_R I_{R0} = (1 - \alpha_R) S_R I_{R0} \end{aligned} \tag{2}$$

Dividing the second set of equations by the first set and rearranging, we get

$$\begin{aligned} \alpha_G &= 1 - \left(\frac{V_G}{V_{G0}}\right) \\ \alpha_R &= 1 - \left(\frac{V_R}{V_{R0}}\right) \end{aligned} \tag{3}$$

By taking the difference, we get

$$\alpha_G - \alpha_R = \frac{V_R}{V_{R0}} - \frac{V_G}{V_{G0}} \tag{4}$$

The binding of the dye to the DNA–PNA duplex results in the shift of the peak from red to green region. This shift can be quantified by the difference ($\alpha_G - \alpha_R$) and can be used to detect the presence of viral RNA (Fig. 3C). We are thus able to reduce the most critical information contained in the entire absorption spectrum of the sample to a two-point absorption measurement only. This results in an enormous simplification of the measurement workflow.

Limit of detection and specificity

We varied the concentration of the purified N1 amplicon and measured the absorbance values both in PortAbs and a plate reader. The amplicons were also visualized by agarose gel electrophoresis (Fig. 4A). As seen in Fig. 4B, the color change due to binding of the $DiSc_2(5)$ dye to the PNA–DNA hybrid could not be distinguished from the NTC by the naked eye for any of the reactions. The ($\alpha_G - \alpha_R$) values for the trimeric complex were also plotted for the spectra obtained from the plate reader (Fig. 4C) and could be distinguished from the NTC only for samples containing at least 74 ng of DNA. In contrast, a Student's t-test confirmed that ($\alpha_G - \alpha_R$) values obtained from PortAbs could be distinguished from the NTC for samples containing as little as 31 ng DNA (Fig. 4D). Thus, the inexpensive and custom-designed PortAbs performed better while detecting lower amounts of DNA using the PNA–$DiSc_2(5)$ method as compared to a commercial plate reader.

Furthermore, we also checked the ability of our system to distinguish SARS-CoV-2 from other respiratory pathogens (Fig. 5). The primers for N1 gene fragment failed to amplify DNA from the genomic DNA of Mtb, the N gene fragment of MERS-CoV and the S gene of SARS-CoV-2. Fig. 5A shows the gel electrophoresis results where an amplicon is only seen for N1 gene of SARS-CoV-2. The ($\alpha_G - \alpha_R$) values for the other samples are comparable to the NTC, as determined by a Student's t-test, while a significant difference is obtained for the N1 gene of SARS-CoV-2 (Fig. 5B). Noticeably, there is no color change in any of the samples that can be distinguished by the naked eye (Fig. 5C). Thus, the detection using PortAbs, in a manner similar to RT-qPCR, depends on the specificity of

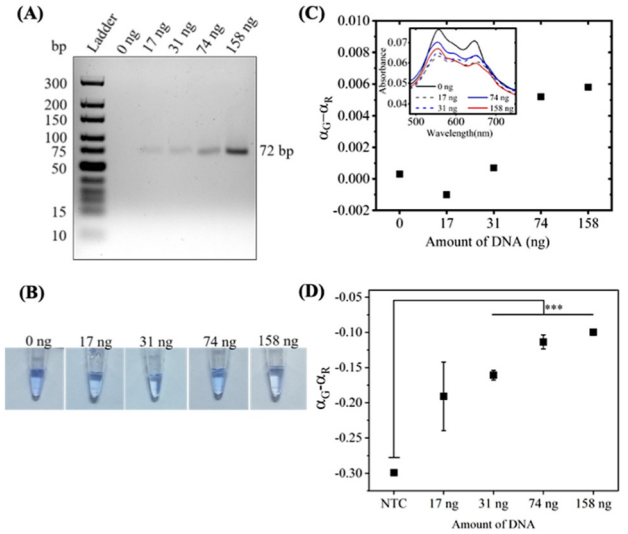

Fig. 4 Testing the sensitivity of detection of the portable device. The CDC-recommended N1 gene fragment was amplified using a control plasmid and successively diluted to determine the limit of detection of the device. (A) Agarose gel image showing the bands corresponding to different dilutions of column-purified PCR product. Varying concentrations of DNA were hybridised with 1 μM PNA and 25 mM $DiSc_2(5)$ as per the protocol described. (B) Color change of the dye after binding to DNA–PNA duplex is not observable to the naked eye. Difference in absorbance of the cyanine dye (C) calculated from the UV-Vis spectra recorded in plate reader (inset) and (D) measured using the portable device, in the presence and absence of DNA–PNA duplex. Statistical significance for the difference between samples was calculated using Student's *t*-test with *** indicating *p*-value < 0.001.

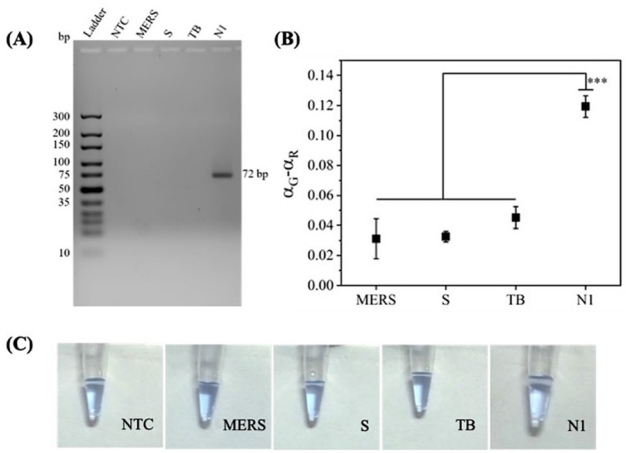

Fig. 5 Depicting the specificity of the detection principle. PCR of MERS-CoV DNA, *M. tuberculosis* (Mtb) DNA, and S and N1 gene segments of SARS-CoV-2 DNA were performed using N1 primers. (A) Agarose gel image showing the primer specificity of the SARS-CoV-2 N1 primers. PCR of MERS-CoV DNA, SARS-CoV-2 spike gene segment and *M. tuberculosis* (Mtb) DNA was performed using N1 primers. (B) Difference in absorbance was measured using the PortAbs system. Statistical significance was calculated using Student's *t*-test with *** indicating *p*-value <0.001. (C) Photographs showing the apparent lack of color change as observed with the naked eye.

the primer-probe sequences used. Since this is a platform technology, it can be easily modified to detect any target nucleic acid.

Validation using COVID-19 clinical specimens

Finally, with the aim of drawing a comparison between the traditional qRT-PCR method and the PortAbs platform, we used clinical samples from patients infected with COVID-19. We tested the ability of the PortAbs methodology to identify SARS-CoV-2 RNA from six clinical samples of patients suffering from COVID-19. The presence of viral RNA was confirmed by RT-qPCR using the CDC-approved N1 primer-probe set (data not shown) as well as using SYBR Green I. All the samples were found to contain SARS-CoV-2 using both qRT-PCR and PortAbs methods. Fig. 6 shows a plot of $(\alpha_G - \alpha_R)$ from PortAbs against the C_t values obtained from SYBR Green based RT-PCR. The C_t values of all samples were below 35, indicating the presence of SARS-CoV-2 (Fig. 6A and B). For the N1 gene, a statistically significant difference was observed between the NTC and all patient samples, confirming the ability of PortAbs to successfully detect SARS-CoV-2 RNA (Fig. 6A). For the sample with the lowest C_t value (P6), the $(\alpha_G - \alpha_R)$ value was found to be the

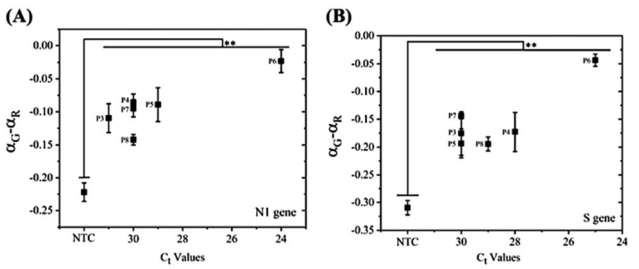

Fig. 6 Validation of the PortAbs methodology using COVID-19 clinical samples. Comparison of C_t values obtained from SYBR Green-based RT-qPCR and $(\alpha_G - \alpha_R)$ values from the PortAbs device for N1 (A) and S gene (B) fragments. All C_t values shown in the plots were obtained using SYBR Green based RT-PCR method. The error bars represent the standard error of mean (SEM) for $(\alpha_G - \alpha_R)$ values. Statistical significance was calculated using the Student's *t*-test and ** indicates *p*-value < 0.01.

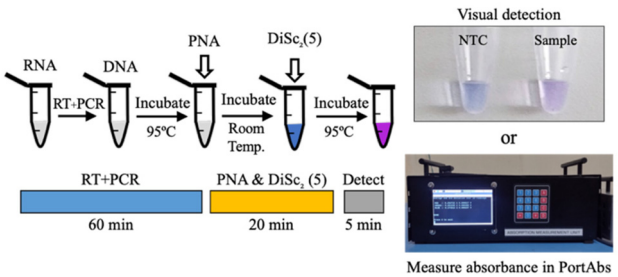

Fig. 7 Complete workflow of PortAbs-based detection. RNA extracted from viral samples is reverse transcribed and amplified by PCR. The color change observed after adding PNA and [$DiSc_2(5)$] can either be visualized with the naked eye, or alternately, the absorption can be measured at 530 nm and 650 nm using the portable measurement platform PortAbs.

highest. In addition to the universally recommended N1, we also checked for the presence of the S gene of SARS-CoV-2 using a complementary PNA sequence. Similar results were obtained for the S gene, with the sample with the highest C_t showing the highest absorbance (Fig. 6B).

The results for S gene confirm that the PortAbs platform can be easily adapted to any target DNA. The only requirement is the design of a highly specific primer set capable of amplifying a conserved portion of the target DNA and a PNA probe that is complementary to the amplified fragment. This simple and low-cost method can be applied for the on-site detection of pathogens without the need for extensive instrumentation.

Conclusions

We present a highly specific method for detection of nucleic acids based on the principle of a cyanine dye, $DiSc_2(5)$, binding to a DNA–PNA hybrid. Our protocol relies on PCR amplification of the target DNA, followed by a rapid purification of the reaction mixture to reduce false-positive signals due to the interaction of the dye with other reaction components. We showed that visual detection of PNA–DNA hybridization based on color change of the dye from blue to purple strongly depends on the concentration of DNA. Such direct detection of specific DNA with the naked eye is difficult and can produce false-negative results when the target DNA concentration is low. With the aid of PortAbs, a two color-absorption platform, we successfully detected as low as 30 ng of the target DNA. Visual detection was inconclusive for DNA amounts ranging from 15 ng to 160 ng. However, absorption values obtained from PortAbs varied linearly with the amount of DNA present in the sample. Finally, we validated our workflow by successfully identifying the signatures of SARS-CoV-2 in six clinical samples with about 1000 copies or more of the viral RNA. In conclusion, we report the development and validation of a protocol for easy, fast, yet specific detection of SARS-CoV-2 RNA using an inexpensive thermal-cycler coupled with a portable, field-deployable, and sensitive absorption detection system, PortAbs. The entire protocol requires less than 90 min (Fig. 7) and can be modified for any target DNA. Our future work will focus on miniaturization of the detection system along with multiplexing of PNA probes for identifying several different targets from the same or different organisms in a single reaction.

Author contributions

Shailesh B. Lad: conceptualization, methodology, investigation, formal analysis, visualization, validation, writing – original draft; Shomdutta Roy: conceptualization, methodology, investigation, formal analysis, visualization, writing – original draft; Jijo Easo George: methodology, investigation, writing – review & editing; Himadri Chakraborti: methodology, investigation, validation; Saumitra Lalsare: methodology, investigation, software; Bikash Barik: methodology, investigation, validation; Arushi Singh: methodology, investigation, validation; Amrutraj Zade: methodology, investigation, writing – review & editing; Sachee Agrawal: methodology, investigation, validation; writing – review & editing; Jayanthi Shastri: methodology, investigation, validation; writing – review & editing; Anirvan Chatterjee: methodology, investigation, validation; writing – review & editing; Kantimay Das Gupta: conceptualization, methodology, supervision, funding acquisition, formal analysis, writing – original draft, writing – review & editing; Debjani Paul: conceptualization, methodology, supervision, funding acquisition, formal analysis, writing – original draft, writing – review & editing; Kiran Kondabagil: conceptualization, methodology, supervision, funding acquisition, project administration, formal analysis, writing – original draft, writing – review & editing.

Ethics statement

The study was approved by the Internal Review Board (Ethics Committee) of the Kasturba Hospital, Mumbai (No. IRB/01/2022 dated 15th February 2022). Patient consent was waived due to screening of retrospective samples (TS/NS) already collected during Covid-19 pandemic. Further samples were anonymized as per the recommendations of the IRB and the "National Guidelines for Ethics Committees Reviewing Biomedical & Health Research During COVID-19 Pandemic", issued by the Indian Council For Medical Research.

Conflicts of interest

There are no conflicts to declare.

Acknowledgements

This work was supported by a grant from the Wadhwani Research Centre for Bioengineering, IIT Bombay [DO/2020-WRCB-0060]. Research in the KK lab was also funded by Science and Engineering Research Board (SERB) grant [RD/0120-SERB000–002]. SL and HC acknowledge IIT Bombay for Ph.D. Fellowship. SR acknowledges DBT funding (RD/0117-DBT0000-013). J. E. G. acknowledges the IIT Bombay postdoctoral fellowship. BB and AS acknowledge DST-INSPIRE and CSIR-UGC, respectively for their Ph.D. research fellowships. We thank Prof. Dinesh Kabra for help with the characterisation of the LEDs.

References

1 M. J. Espy, J. R. Uhl, L. M. Sloan, S. P. Buckwalter, M. F. Jones, E. A. Vetter, J. D. C. Yao, N. L. Wengenack, J. E. Rosenblatt, F. R. Cockerill and T. F. Smith, *Clin. Microbiol. Rev.*, 2006, **19**, 595–595.

2 V. M. Corman, O. Landt, M. Kaiser, R. Molenkamp, A. Meijer, D. K. W. Chu, T. Bleicker, S. Brünink, J. Schneider, M. L. Schmidt, D. G. J. C. Mulders, B. L. Haagmans, B. Van Der Veer, S. Van Den Brink, L. Wijsman, G. Goderski, J. L. Romette, J. Ellis, M. Zambon, M. Peiris, H. Goossens, C. Reusken, M. P. G. Koopmans and C. Drosten, Detection of 2019 novel coronavirus (2019-nCoV) by real-time RT-PCR, *Eurosurveillance*, 2020, **25**, 23–30.

3 X. Lu, L. Wang, S. K. Sakthivel, B. Whitaker, J. Murray, S. Kamili, B. Lynch, L. Malapati, S. A. Burke, J. Harcourt, A. Tamin, N. J. Thornburg, J. M. Villanueva and S. Lindstrom, *Emerging Infect. Dis.*, 2020, **26**, 1654–1665.

4 M. J. Kellner, J. G. Koob, J. S. Gootenberg, O. O. Abudayyeh and F. Zhang, *Nat. Protoc.*, 2019, **14**, 2986–3012.

5 M. Azhar, R. Phutela, M. Kumar, A. H. Ansari, R. Rauthan, S. Gulati, N. Sharma, D. Sinha, S. Sharma, S. Singh, S. Acharya, S. Sarkar, D. Paul, P. Kathpalia, M. Aich, P. Sehgal, G. Ranjan, R. C. Bhoyar, K. Singhal, H. Lad, P. K. Patra, G. Makharia, G. R. Chandak, B. Pesala, D. Chakraborty and S. Maiti, Rapid and accurate nucleobase detection using FnCas9 and its application in COVID-19 diagnosis, *Biosens. Bioelectron.*, 2021, **183**, 113207.

6 J. P. Broughton, X. Deng, G. Yu, C. L. Fasching, V. Servellita, J. Singh, X. Miao, J. A. Streithorst, A. Granados, A. Sotomayor-Gonzalez, K. Zorn, A. Gopez, E. Hsu, W. Gu, S. Miller, C. Y. Pan, H. Guevara, D. A. Wadford, J. S. Chen and C. Y. Chiu, *Nat. Biotechnol.*, 2020, **38**, 870–874.

7 Z. Li, Y. Yi, X. Luo, N. Xiong, Y. Liu, S. Li, R. Sun, Y. Wang, B. Hu, W. Chen, Y. Zhang, J. Wang, B. Huang, Y. Lin, J. Yang, W. Cai, X. Wang, J. Cheng, Z. Chen, K. Sun, W. Pan, Z. Zhan, L. Chen and F. Ye, *J. Med. Virol.*, 2020, **92**, 1518–1524.

8 J. Xiang, M. Yan, H. Li, T. Liu, C. Lin, S. Huang and C. Shen, medRxiv, 2020, 2020.02.27.20028787.

9 R. Funari, K. Y. Chu and A. Q. Shen, *Biosens. Bioelectron.*, 2020, **169**, 112578.

10 P. E. Nielsen, M. Egholm, R. H. Berg and O. Buchardt, *Science*, 1991, **254**, 1497–1500.

11 M. Egholm, O. Buchardt, P. E. Nielsen and R. H. Berg, *J. Am. Chem. Soc.*, 1992, **114**, 1895–1897.

12 T. T. Nikiforov and S. Jeong, *Anal. Biochem.*, 1999, **275**, 248–253.

13 J. O. Smith, D. A. Olson and B. A. Armitage, *J. Am. Chem. Soc.*, 1999, **121**, 2686–2695.

14 B. A. Armitage, in *Topics in Current Chemistry*, 2005, vol. 253, pp. 55–76.

15 M. Komiyama, S. Ye, X. Liang, Y. Yamamoto, T. Tomita, J.-M. Zhou and H. Aburatani, *J. Am. Chem. Soc.*, 2003, **125**, 3758–3762.

16 L. M. Wilhelmsson, B. Nordén, K. Mukherjee, M. T. Dulay and R. N. Zare, *Nucleic Acids Res.*, 2002, **30**, 3–6.

17 T. Tedeschi, S. Sforza, S. Ye, R. Corradini, A. Dossena, M. Komiyama and R. Marchelli, *J. Biochem. Biophys. Methods*, 2007, **70**, 735–741.

18 J. Duy, R. L. Smith, S. D. Collins and L. B. Connell, *Biosens. Bioelectron.*, 2014, **52**, 433–437.

19 G. Papadakis, A. K. Pantazis, N. Fikas, S. Chatziioannidou, V. Tsiakalou, K. Michaelidou, V. Pogka, M. Megariti, M. Vardaki, K. Giarentis, J. Heaney, E. Nastouli, T. Karamitros, A. Mentis, A. Zafiropoulos, G. Sourvinos, S. Agelaki and E. Gizeli, *Sci. Rep.*, 2022, **12**, 1–15.

20 G. S. Luka, E. Nowak, Q. R. Toyata, N. Tasnim, H. Najjaran and M. Hoorfar, *Sci. Rep.*, 2021, **11**, 1–12.

21 M. Xu, P. Fu, S. Xing, Y. Zhao and C. Zhao, *ChemBioChem*, 2020, **21**, 2667–2675.

22 M. Wang, R. Holmes-Davis, Z. Rafinski, B. Jedrzejewska, K. Y. Choi, M. Zwick, C. Bupp, A. Izmailov, J. Paczkowski, B. Warner and H. Koshinsky, *Anal. Chem.*, 2009, **81**, 2043–2052.

23 J. Duy, R. L. Smith, S. D. Collins and L. B. Connell, *Am. J. Potato Res.*, 2015, **92**, 398–409.

24 J. Duy, R. L. Smith, S. D. Collins and L. B. Connell, in *OCEANS'11 MTS/IEEE KONA*, IEEE, 2011, pp. 1–5.

25 M. K. Cichon, C. H. Haas, F. Grolle, A. Mees and T. Carell, *J. Am. Chem. Soc.*, 2002, **124**, 13984–13985.